Inorganic Chemistry

Article

pubs.acs.org/IC

New Approach for the Step by Step Control of Magnetic Nanostructure Functionalization

P. Riani,[†,‡] M. A. Lucchini,*[,†] S. Thea,[†] M. Alloisio,[†] G. Bertoni,[§] and F. Canepa[†,∥]

[†]Department of Chemistry and Industrial Chemistry, University of Genoa, Via Dodecaneso 31, 16146 Genoa, Italy

[‡]INSTM-UDR Genoa, Via Dodecaneso 31, 16146 Genoa Italy

[§]IMEM-CNR, Parco Area delle Scienze 37/A, 43124 Parma, Italy

[∥]SPIN-CNR, Corso Perrone 24, 16152 Genoa, Italy

Supporting Information

ABSTRACT: This paper describes the synthesis, functionalization, and multitechnique analysis of magnetic nanoparticles. The synthetic method involves the covering of a magnetite nucleus by a silica layer and the further functionalization with different fluorophores via a cross-linker molecule. All synthetic intermediates were analyzed by fluorescence spectroscopy and AC magnetic susceptibility. For one of the considered molecules, a further investigation with STEM, EDXS, and DLS has been conducted in order to validate the proposed magnetic results. The comparison between the two techniques is used to ensure a complete characterization of the product confirming the success of the synthesis. By comparing the magnetic and the fluorescence measurements, we also demonstrate the effectiveness of AC susceptibility as a robust and versatile technique to follow the synthesis of complex magnetic nanostructures regardless of the nature of the functionalization.

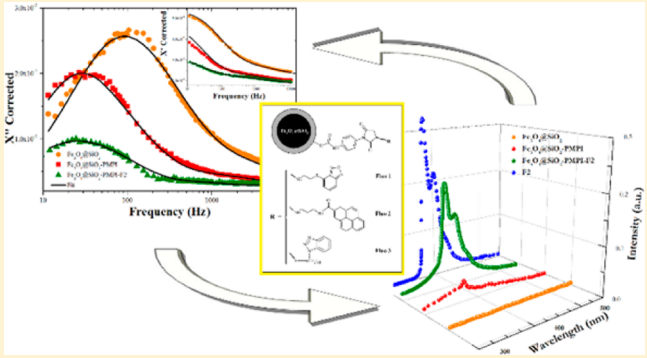

1. INTRODUCTION

Engineered nanoparticles (NPs) offer a wide range of potentially useful technological applications, ranging from industrial uses (heterogeneous catalysis, superplastic materials, self-cleaning building surfaces),[1−4] to the environment and renewable energy (wastewater treatment, catalysis, Li ion battery electrodes),[5−8] to medical and health care applications (UV protection, drug delivery, imaging, cancer therapy).[9−15] Further improvements can be achieved by combining different physical properties in a single nanostructure (multifunctionalization) leading to new classes of nanomaterials.

The synthesis of magnetic nanoparticles coated with fluorescent molecules offers the possibility to obtain a magnetically driven nanoscale photonic device that can be employed for in vitro and in vivo bioimaging applications.[16] Furthermore, an additional functionalization with a specific drug can lead to a new class of all-in-one diagnostic and therapeutic tools, i.e., visualization and, at the same time, treatment of different diseases.[17,18] However, the complete physical characterization, also from a dimensional point of view, is fundamental for the development of this field. Dynamic light scattering (DLS) is the method typically used for the characterization of NPs in solution, but it has some disadvantages: (i) it has low resolution, i.e., particles must differ in size by 50% or more to reliably result in two well-defined peaks by DLS; (ii) the signal of a small quantity of small NPs can be easily covered by the signal from a few larger NPs; (iii) the signal can be strongly affected by other species or impurities present in the solution, giving information not related to the sample under investigation.

Typically, magnetic nanoparticles (MNPs) in suspension subjected to an alternate magnetic field show two different relaxation mechanisms: the Brownian and the Néel ones. Recently, a physicomathematical model based on the above-mentioned relaxations has been developed in our group.[19] In our previous work we demonstrated the effectiveness of the proposed method to successfully characterize silica coated magnetite nanoparticles (Fe_3O_4@SiO_2) in suspension. This analysis (a) is nondestructive, (b) can be used in each step of the functionalization, (c) allows simultaneous acquisition of multiple information, (d) is performed on a very small amount of suspension (about 200 μL), and (e) is not affected by the presence of nonmagnetic impurities.

The proposed method is used in this Article to verify the success of the three step functionalization of magnetite nanoparticles with different fluorescent molecules. In order to validate the proposed method, we compared the magnetic results with scanning transmission electron microscopy (STEM), fluorescence spectroscopy, and DLS results. The

Received: May 22, 2014
Published: August 20, 2014

   dx.doi.org/10.1021/ic501194n | Inorg. Chem. 2014, 53, 9166−9173

complete characterization has been conducted on a single molecule, and once the consistency of the techniques was verified, just AC susceptometry and spectrofluorimetry have been used for the other molecules.

These three functionalizations can be described as (1) an inorganic coating of silica (SiO_2), (2) a cross-linker molecule [*N*-(*p*-maleimidophenyl)-isocyanate (PMPI)], and, finally, (3) different fluorescent molecules, endowed with different reacting groups, sizes of the fluorophore moieties, and lengths of the intervening chains.

By using various fluorescent molecules, we demonstrated the possibility to bond organic molecules with different chemical (amines, thiols) and morphological characteristics (length of the chain) in the final step. The three fluorescent molecules used in this work are 22-(benzofurazan-4-thio)ethylamine (Fluo1), *N*-(3-aminopropyl) pyrene-1-carboxamide (Fluo2), and 11-benzotriazol-1′-yl-undecane-1-thiol (Fluo3). To our knowledge, this is the first time that all the different stages of the functionalization process are quantitatively analyzed by means of dynamic magnetic measurements in terms of changes of the dimensions of the NPs. Each magnetic information was successfully supported by at least the results of the fluorescence spectra.

2. EXPERIMENTAL SECTION

2.1. Materials. *N*-(*p*-Maleimidophenyl)-isocyanate was supplied by Thermo Scientific (Thermo Fisher Scientific Inc.). All other reagents (either organic or inorganic) and solvents were purchased from Sigma-Aldrich and used as received. Fluorescent molecules Fluo1 and Fluo2 were synthesized as described below. Synthesis of Fluo3 had been already reported in the literature.[20]

2.2. Methods. NMR spectra were recorded using a Varian Gemini 300 operating at 300 MHz (^{1}H) or 75 MHz (^{13}C).

To assess the elemental composition of compounds Fluo1 and Fluo2, high resolution mass spectrometry (HRMS) analyses were performed in direct infusion analysis (DIA) in reflection positive ion mode on a 6210 time of flight mass spectrometer (Agilent, Santa Clara, CA) coupled with an electrospray ion source (ESI). The calculations were performed using a utility integrated in the dedicated software, and the calculated elemental formulas were unambiguous for both compounds. The spectra obtained from NMR as well as from HRMS are collected in the Supporting Information.

The morphology of the Fe_3O_4@SiO_2 MNPs was assessed by field emission scanning electron microscopy (FE-SEM; ZEISS SUPRA 40 VP) equipped with an energy dispersive X-ray spectrometer (EDXS-OXFORD "INCA Energie 450x3") for microanalysis.

Transmission electron microscopy images were acquired on a JEOL JEM-2200FS microscope with a Schottky emitter at 200 kV, operated in scanning mode with a high angle annular dark field detector (STEM-HAADF) using an inner cutoff angle of 75 mrad and a 0.5 nm probe size. A 1.0 nm probe size was used for energy dispersive X-ray spectroscopy (EDXS) to improve the signal-to-noise ratio in the spectra. Note that a Cu signal is always present in the EDX spectra, and deriving from the copper grid of the supporting film.

Dynamic light scattering data were obtained with a Zetasizer Nano S dynamic light scattering (DLS) instrument (Malvern Instruments, Malvern, U.K.) setting the appropriate viscosity and refractive index parameters for each solution and keeping the temperature at 20 °C during the measurements by means of a Peltier thermostating system. Samples were prepared diluting the particles in the appropriate solvent [water or dimethyl sulfoxide (DMSO)] and obtaining a final concentration of about 0.2 mg/mL. The suspensions were sonicated in an ultrasonic bath for 5 min before the analyses.

Fluorescence measurements were performed by means of a PerkinElmer MPF-44A fluorescence spectrophotometer with 150 W xenon bulb.

The AC susceptibility measurements were obtained using an OXFORD Maglab^{2000} magnetic measurements system operating in the $1-10^4$ Hz frequency range with an AC magnetic field of 10 Oe. The resolution of the AC signal was better than 10^{-7} emu.

2.3. Synthetic Procedures. *2.3.1. Synthesis of 2-(Benzofurazan-4-thio)ethylamine (Fluo1).* To a solution of 4-fluoro-2,1,3-benzoxadiazole (1.5 g, 10.9 mmol) in anhydrous ethanol (EtOH, 10 mL) placed in a 100 mL three-necked round-bottom flask equipped with a dropping funnel and a magnetic stirrer, a solution of cysteamine hydrochloride (1.64 g, 10.9 mmol) in ethanolic sodium ethoxide [obtained dissolving Na (0.5 g, 21.8 mmol) in anhydrous EtOH (20 mL)] was added dropwise under nitrogen with mild heating. After stirring for 2 h, the so-obtained yellow mixture was filtered and poured into water (150 mL), the solution was brought to pH 2 by addition of 4% (v/v) HCl, and repeatedly extracted with diethyl ether (Et_2O). Following this, 10% (v/v) NaOH was added to the aqueous phase up to pH 12, the aqueous phase was extracted with Et_2O, and the organic layer was dried over Na_2SO_4 and concentrated in vacuo to give 1.68 g (79% yield) of Fluo1 as an orange solid (mp 90.0−90.6 °C).

^{1}H NMR (300 MHz, $CDCl_3$) δ = 7.63 (dd, J = 8.8, 0.8 Hz, 1H), 7.33 (dd, J = 8.8, 6.9 Hz, 1H), 7.25 (dd, J = 6.8, 0.8 Hz, 1H), 3.31 (t, J = 6.3 Hz, 2H), 3.03 (t, J = 6.4 Hz, 2H). ^{13}C NMR (75 MHz, $CDCl_3$) δ = 149.46, 149.38, 131.75, 127.91, 127.18, 113.24, 41.06, 36.29. HRMS (ESI-TOF) m/z calcd for $C_8H_{10}N_3OS$: 196.054 46 $[M + H]^+$; found: 196.057 61.

2.3.2. Synthesis of N-(3-Aminopropyl)pyrene-1-carboxamide (Fluo 2). In a 100 mL round-bottom flask flushed with dry nitrogen immersed in an ice bath, a solution of 1-pyrenecarboxylic acid (0.5 g, 2.03 mmol) in dimethylformamide (DMFA, 3.0 mL) was added to 2-(1*H*-benzotriazole-1-yl)-1,1,3,3-tetramethyluronium hexafluorophosphate (1.54 g, 4.06 mmol) dissolved in DMFA (5 mL) under magnetic stirring. *N*,*N*-Diisopropyethylamine (0.8 mL, 4.06 mmol) was then added to the mixture, which gave rise to formation of a yellow precipitate. After 1 h the ice bath was removed and a solution of *N*-Boc-1,3-propanediamine (0.42 g, 2.44 mmol) in 1 mL of DMFA was added, which led to formation of a brownish, clear solution. After 1 h the reaction mixture was poured into 50 mL of water and repeatedly extracted with CH_2Cl_2; the organic phase was washed with 4% (v/v) HCl and finally with 5 wt % $NaHCO_3$. Pure *N*-Boc protected Fluo2 was obtained by flash column chromatography on silica gel (eluent ethyl acetate (EtOAc)/CH_2Cl_2 3:7) as a white solid (0.73 g, 89.3% yield), and used as such in the subsequent reaction. *N*-Boc protected Fluo2 (0.73 g, 1.8 mmol) was suspended in anhydrous dichloromethane (13 mL) at 0 °C. Trifluoroacetic acid (13 mL) was subsequently added, quickly yielding a clear, bright yellow solution. After 1 h the cooling bath was removed; after an extra 2 h at room temperature, the solvent was rotoevaporated under reduced pressure. The solid residue was then washed repeatedly with a hexane−dichloromethane mixture (1:1), the product was dissolved into 5 wt % $NaHCO_3$, the aqueous solution was extracted several times with CH_2Cl_2 and EtOAc, and the organic phase was washed with water and dried over Na_2SO_4. Crystallization from toluene gave a light yellow solid (0.25 g, 46% yield, mp 147−149 °C).

^{1}H NMR (300 MHz, DMSO-d_6): δ = 8.74 (br t, J = 5.1 Hz, 1H), 8.48 (d, J = 9.3 Hz, 1H), 8.34 (m, 3H), 8.24 (m, 3H), 8.12 (m, 2H), 3.47 (m, 2H), 3.1 (br s, 2H), 2.72 (t, J = 6.7 Hz, 2H), 1.72 (quint, J = 6.7 Hz, 2H). ^{13}C NMR (75 MHz, DMSO-d_6): δ = 168.81, 132.25, 131.47, 130.71, 130.20, 128.20, 128.05, 127.71, 127.20, 126.56, 125.76, 125.56, 125.13, 124.66, 124.41, 123.79, 123.65, 38.8 (from gHSQC), 37.12, 32.81. HRMS (ESI-TOF) m/z calcd for $C_{20}H_{19}N_2O$: 303.149 75 $[M + H]^+$; found: 303.155 99.

2.3.3. Synthesis of the Inorganic Nucleus (Fe_3O_4@SiO_2). Magnetite nanoparticles were obtained by the coprecipitation method from an aqueous solution of stoichiometric amounts of $FeCl_2{\cdot}4H_2O$ and $FeCl_3{\cdot}6H_2O$ under basic conditions. Details of the sample preparation are reported elsewhere.[21] Briefly, $FeCl_2{\cdot}4H_2O$ (2.5 mmol) and $FeCl_3{\cdot}6H_2O$ (5 mmol) were dissolved in Milli-Q water at pH 2 under N_2 atmosphere and vigorous mechanical stirring. Once the solution reached 75 °C, a proper amount of NH_3 aqueous solution (28 wt %) was quickly added, causing a sudden appearance of a black color in the

dx.doi.org/10.1021/ic501194n | Inorg. Chem. 2014, 53, 9166−9173

solution. The reaction was continued for 15 min, after which the particles were washed several times with boiling water using a magnetic collection after each wash.

The magnetite nanoparticles were coated with silica by hydrolysis and condensation following a modified Stober process[22] using tetraethylorthosilicate (TEOS, 98 wt %) at 40 °C.[19] Usually, an aqueous suspension of magnetite particles at the concentration of 60 mg/L was placed in a three-necked flask at 40 °C diluted with ethanol (200 mL) and ultrasonicated for 15 min. To this suspension, water (4 mL), NH_3 28% aqueous solution (9 mL) and TEOS (1.2 mL) were added in sequence. The as-prepared suspension was then maintained under reaction conditions for 2 h. Finally, Fe_3O_4@SiO_2 was collected using a magnetic separation in order to avoid the collection of nonmagnetic silica spheres. The as-collected particles were washed at least three times, always using a static magnetic field for the separation from the solution. Once washed the sample was stored as a suspension in water.

2.3.4. Reaction with N-(p-Maleimidophenyl)-isocyanate. The reaction between silica coated nanoparticles and *N*-(*p*-maleimidophenyl)-isocyanate (PMPI) occurs at room temperature (RT) in anhydrous dimethyl sulfoxide (DMSO). Fe_3O_4@SiO_2 NPs (in aqueous solution) were centrifuged at 14 000 rpm for 15 min and washed several times with anhydrous DMSO in order to completely remove the water, a necessary step to prevent the fast hydrolysis of the isocyanate group of PMPI. PMPI (DMSO solution) was added to the NPs in anhydrous DMSO, and the suspension was vigorously stirred at RT for 2 h. Finally, the solution was washed by centrifugation several times to completely eliminate the PMPI excess and again dispersed in DMSO.

2.3.5. Addition of Fluorophores. The maleimido group reacts selectively with thiols at RT and at pH ranging from 6.5 to 7.5, while reaction with amines requires a pH higher than 9 and a temperature between 330 and 350 K.[23] For each fluorescent molecule, a solution in anhydrous dimethyl sulfoxide (DMSO) was prepared at room temperature. The Fe_3O_4@SiO_2@PMPI NPs, dispersed in DMSO, were then mixed with an excess of the fluorescent molecule in DMSO, reaching a total volume of 2 mL. The vial was then placed in a thermo mixer with vigorous shaking under time and temperature conditions depending on the fluorescent molecule. The final product was then washed again with DMSO several times to completely remove the excess of unreacted fluorescent molecules, and stored in fresh DMSO. The sketch of the final structure of the functionalized magnetic nanoparticles with the three different fluorescent molecules is reported in Figure 1.

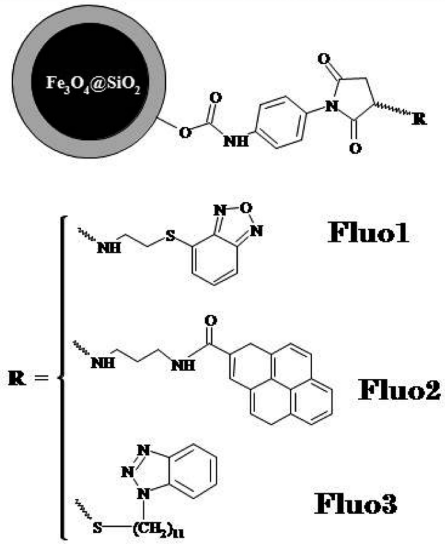

Figure 1. Sketch of functionalized magnetite nanoparticles with different fluorescent molecules.

3. RESULTS

In Figure 2a a FESEM image of Fe_3O_4@SiO_2 nanoparticles is presented. EDXS analysis (reported in Figure 2c) collected from a single particle confirms the presence of the expected elements in the structures, namely iron, silicon, and oxygen. The core−shell nature of the particles is well visible in the HAADF-STEM image (Figure 2b) thanks to the compositional contrast; magnetite (heavier) appears brighter than silica (lighter).

Every functionalization with a different fluorescent molecule has been carried out starting from different samples of Fe_3O_4@SiO_2. Despite the different batches, each sample showed the same chemical and morphological characteristics.

3.1. Functionalization with the Fluo1 Molecule. The intermediates involved in the functionalization with the molecule Fluo1 have been analyzed both by the proposed magnetic method and by more conventional techniques such as STEM, EDXS, DLS, and spectrofluorimetry. These last techniques are typically used to investigate this kind of system, and we considered them to validate the proposed magnetic model in a multistep synthesis.

Figure 3 shows the fluorescence spectra performed on the three different intermediates, namely Fe_3O_4@SiO_2, Fe_3O_4@SiO_2@PMPI, and Fe_3O_4@SiO_2@PMPI@Fluo1 together with that of the free Fluo1 molecule. All particles and the fluorescent molecule are dispersed in DMSO.

The fluorophore alone displays two small peaks around 372 and 392 nm, followed by a very large emission at 494 nm. As expected, no fluorescence signal is detected for the silica coated magnetic NPs. The PMPI in DMSO presents a very large peak around 380 nm with a maximum centered at 373 nm. Similarly, a small peak is observed at 372 nm in the PMPI-functionalized NPs. This peak can be assigned to the maleimidophenyl moiety of the cross-linker, and it has been considered as evidence of the presence of PMPI on the NP surface. The comparison between the two spectra is reported as the inset in Figure 3. After the addition of the Fluo1 molecule to the NPs, two novel emission peaks are shown at 372 and 393 nm, respectively. These two peaks present the same wavelengths of the high-energy bands of the free fluorophore, confirming the anchoring of the photoactive molecule. Of notice is the absence of the main emission around 500 nm whose ratio with the high energy peaks has been found to be strongly related to the dye concentration, and it increases at higher concentrations (see Supporting Information). This evidence, combined with the absence of the peak at 500 nm, suggests a low loading of Fluo1 in the final product.

In Figure 4a the STEM image of the final adduct (Fe_3O_4@SiO_2@PMPI@Fluo1) is shown, and the corresponding EDX spectrum is reported in Figure 4b. The image suggests that the functionalization does not affect the morphology of the inorganic nucleus, and EDXS confirms the presence of the organic molecules thanks to the presence of the S peak. In the spectrum, the presence of nitrogen cannot be observed probably because the N peak is covered by the tail of the strong O peak coming from the silica coating.

The complex susceptibility has been measured at room temperature for the different intermediates: Fe_3O_4, Fe_3O_4@SiO_2, Fe_3O_4@SiO_2@PMPI, and Fe_3O_4@SiO_2@PMPI@Fluo1. The data were corrected by the contribution of the solvent.[24] Figure 5 shows the imaginary component (χ''), while in the

dx.doi.org/10.1021/ic501194n | Inorg. Chem. 2014, 53, 9166−9173

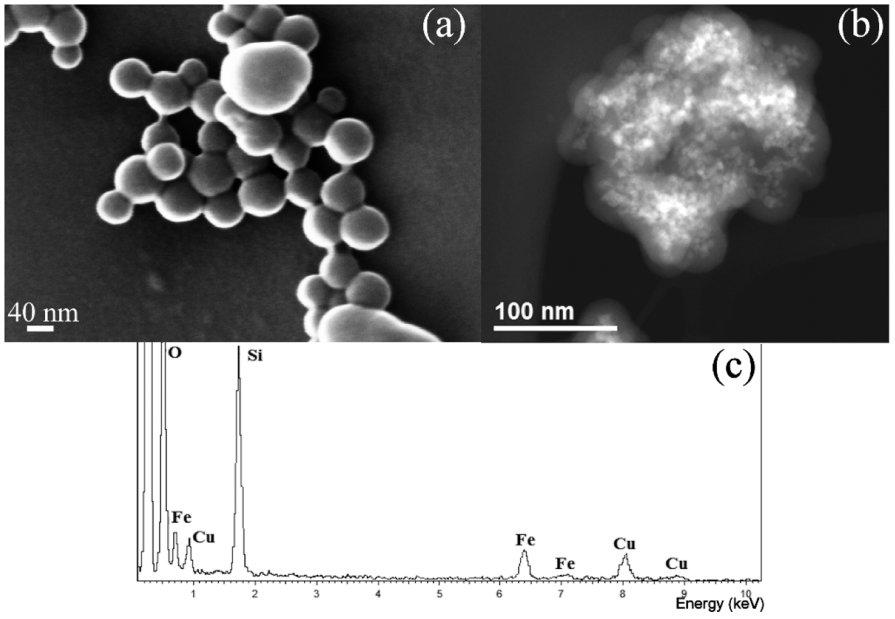

Figure 2. (a) FESEM image of Fe_3O_4@SiO_2 nanoparticles with (b) HAADF-STEM image (magnetite brighter than the silica coating) and (c) related EDX spectrum.

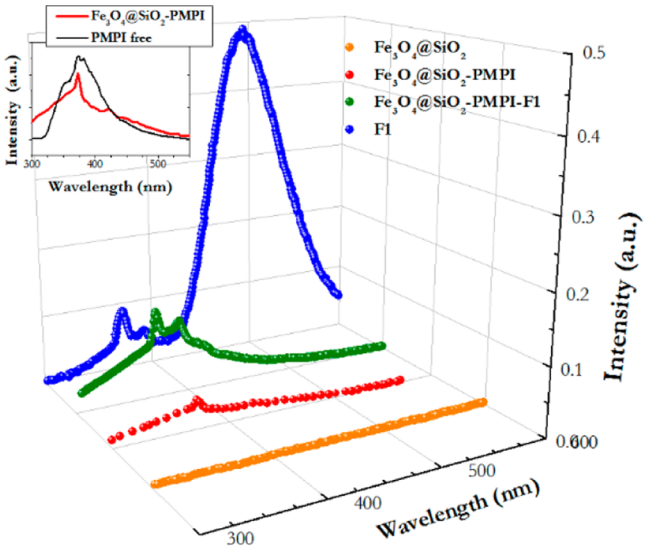

Figure 3. Fluorescence spectra of different intermediates involved in functionalization with the Fluo1 (F1) molecule. In the inset, the comparison of the spectra of the free PMPI and the PMPI bonded to the silica surface of the NP is presented.

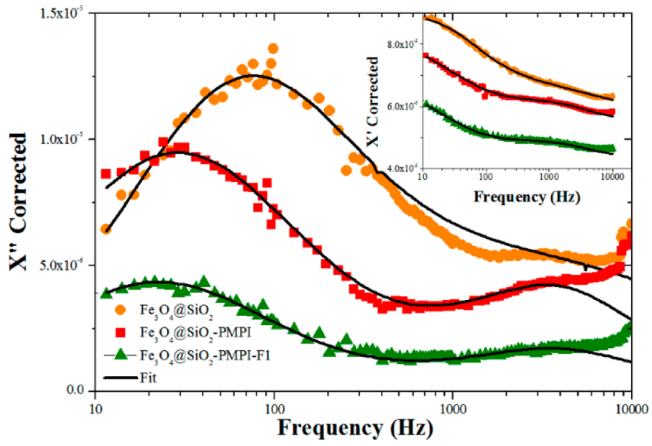

Figure 5. Imaginary component of the AC magnetic susceptibility of the three step functionalization of the NPs with the Fluo1 (F1) fluorophore: ●, Fe_3O_4@SiO_2; ■, Fe_3O_4@SiO_2@PMPI; ▲, Fe_3O_4@SiO_2@PMPI@F1. In the inset, the real component is presented. The fits obtained from the physicomathematical model presented in the text are shown as solid lines.

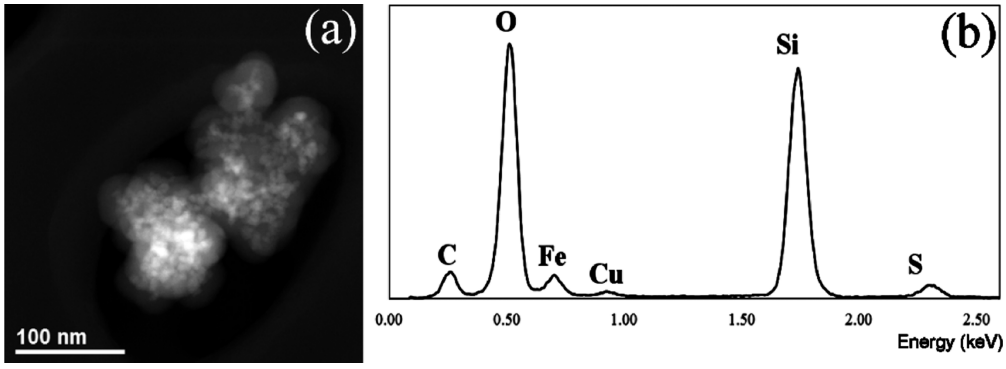

Figure 4. (a) HAADF-STEM image of Fe_3O_4@SiO_2@PMPI@Fluo1 and (b) corresponding EDX spectrum.

dx.doi.org/10.1021/ic501194n | Inorg. Chem. 2014, 53, 9166−9173

inset the frequency dependence of the real component (χ') is depicted.

χ' exhibits in the three steps a similar trend with a decreasing behavior at increasing frequency. The behavior of the imaginary component is also meaningful: in the three functionalization steps a well-defined maximum at relatively low frequencies is observed with a decreasing of the peak frequency related to an increasing in the thickness of the functionalization (see the section Magnetic Model).The increasing of the dimension of the intermediates is observed also by DLS measurements: we obtained a mean radius value of 114 nm [polydispersity index (PDI) 0.133] for Fe_3O_4@SiO_2, 116 nm (PDI 0.114) for Fe_3O_4@SiO_2@PMPI, and, finally, 124 nm (PDI 0.217) for Fe_3O_4@SiO_2@PMPI@Fluo1.

3.2. Functionalization with the Fluo2 Molecule. Figure 6 shows the fluorescence spectra referring to the three

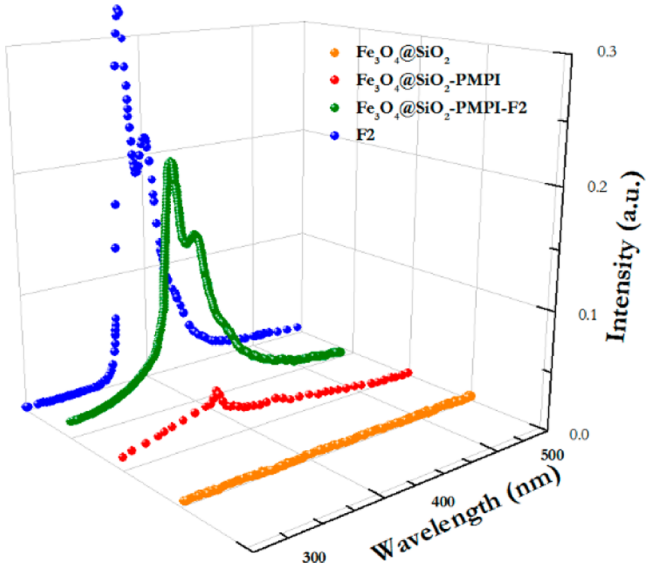

Figure 6. Fluorescence spectra of different intermediates involved in functionalization with the Fluo2 (F2) molecule.

progressive coatings of the Fe_3O_4 NPs with the molecule Fluo2 (SiO_2, SiO_2@PMPI, and SiO_2@PMPI@Fluo2) and to the free fluorophore dissolved in DMSO. Again, whereas the Fe_3O_4@SiO_2 fluorescence signal is zero, the presence of the PMPI is detected by the appearance of the weak emission at 373 nm.

The subsequent coating with the Fluo2 molecule matches the comparison of two clear peaks at 384 and 402 nm, completely overlapping those found in the spectrum of the dye molecule alone. The peaks correspond to the typical band I and band III of the monomer form of pyrene rings.[25] The unchanged position before and after the anchoring to the NP surface indicates that no interactions occurred at the excited state between the components of the nanohybrid. Moreover, also the intensity ratio of peak III to peak I ($I_{III/I}$) is found to be not affected by the functionalization reaction. Since the $I_{III/I}$ parameter is commonly used to sense microenvironmental properties,[26] this result denotes that the local environments close to the NP surface have the same polarity as the bulk solvent medium.

In Figure 7 the real (inset) and imaginary components of the complex susceptibility are reported as a function of the frequency at room temperature. The trends of χ' (a continuous

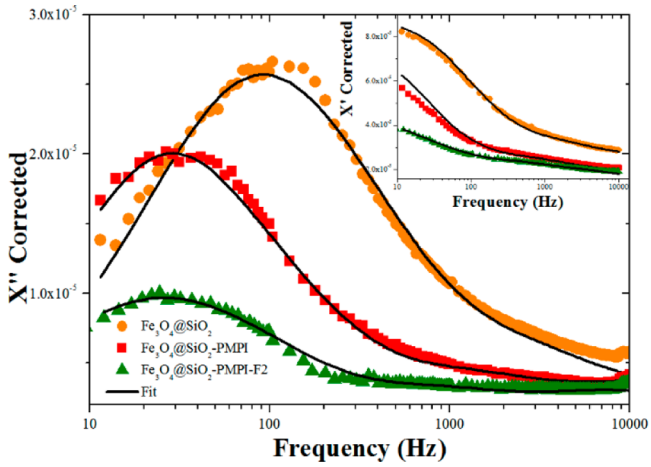

Figure 7. Imaginary component of the AC magnetic susceptibility of the three step functionalization of the NPs with the Fluo2 (F2) fluorophore: ●, Fe_3O_4@SiO_2; ■, Fe_3O_4@SiO_2@PMPI; ▲, Fe_3O_4@SiO_2@PMPI@F2. In the inset, the real component is presented. The fits obtained from the physicomathematical model presented in the text are shown as solid lines.

decrease with the frequency) and χ'' (a well-defined maximum at different frequencies for the progressive coatings) are qualitatively very similar to those presented for the functionalization of the Fluo1 molecule.

3.3. Functionalization with the Fluo3 Molecule. Figure 8 displays the fluorescence spectra of the progressive coatings

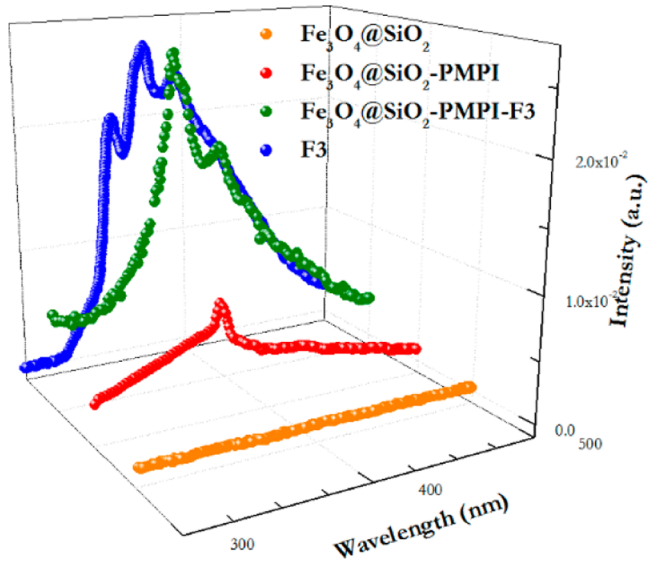

Figure 8. Fluorescence spectra of different intermediates involved in functionalization with the Fluo3 (F3) molecule.

of magnetite NPs with Fluo3 (SiO_2, SiO_2@PMPI, and SiO_2@PMPI@Fluo3) compared with the spectrum of the free dye in the same solvent. Molecule Fluo3 exhibits an emission profile characterized by three distinct peaks at 356, 377, and 396 nm, respectively. The spectra of the Fe_3O_4@SiO_2 and Fe_3O_4@SiO_2@PMPI NPs are very similar to those observed for the functionalization with Fluo1 and Fluo2. After the reaction with Fluo3, we observe a slightly different emission profile composed by a peak centered at 372 nm with an associated

dx.doi.org/10.1021/ic501194n | Inorg. Chem. 2014, 53, 9166−9173

shoulder at 378 nm, followed by a second peak centered at 398 nm.

In Figure 9, χ' and χ'' are displayed as a function of the frequency for the different steps of the functionalization. Again,

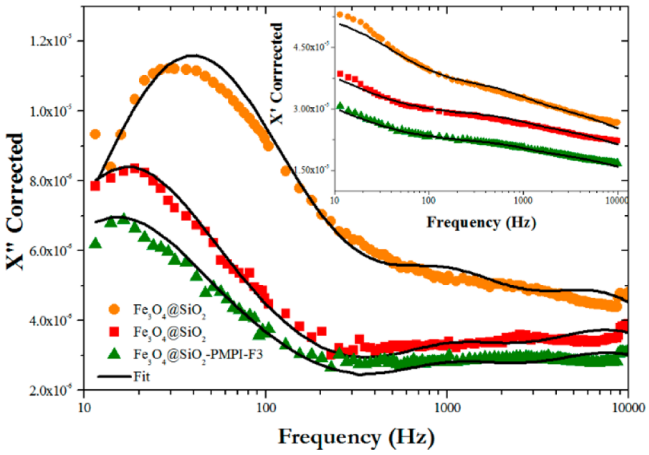

Figure 9. Imaginary component of the AC magnetic susceptibility of the three step functionalization of the NPs with the Fluo3 (F3) fluorophore: ●, Fe_3O_4@SiO_2; ■, Fe_3O_4@SiO_2@PMPI; ▲, Fe_3O_4@SiO_2@PMPI@F3. In the inset, the real component is presented. The fits obtained from the physicomathematical model presented in the text are shown as solid lines.

a decreasing behavior for the real susceptibility resulting for the progressive coatings is observed, while broad maxima are displayed in the imaginary component at 34, 17, and 13 Hz for the Fe_3O_4@SiO_2, Fe_3O_4@SiO_2@PMPI, and Fe_3O_4@SiO_2@PMPI@Fluo3 coatings, respectively.

4. MAGNETIC MODEL

Our functionalized magnetic NPs typically present a magnetic core composed by one or more superparamagnetic (single domain) magnetite nanoparticles surrounded by an inorganic shell (SiO_2) able to interact with organic molecules through the hydroxyl groups on its surface. Organic (fluorescent) molecules are attached to the surface by chemical bonds.

When an AC magnetic field is applied, the behavior of these functionalized NPs in solution is characterized by two different relaxation mechanisms related to the alignment of the magnetic vector of the NP with the direction of the AC field. The Néel mechanism[27] is related to the rotation of the magnetization vector of the NP without any physical rotation of the single domain. This relaxation depends on the magnetic anisotropy constant K of the NP, the volume V of the single domain, and the temperature T through the relation

$$\tau = \tau_0 \exp\left(\frac{KV}{k_B T}\right) \tag{1}$$

Here τ_0 is a constant parameter with typical values ranging between 10^{-9} and 10^{-13} s and k_B is the Boltzmann constant.

On the other side, the Brownian relaxation[28] corresponds to the rotation of the whole NP together with solvent molecules interacting with the surface. In this case the relaxation time depends on the temperature and viscosity η of the solvent and on the physical volume of the NP (comprising also the hydration molecules) following the equation

$$\tau_B = \frac{4\pi\eta r_{hydr}^{\ 3}}{k_B T} \tag{2}$$

where r_{hydr} is the hydrodynamic radius of the NP (under the hypothesis of a spherical shape).

In the framework of the Debye model,[29,30] the isothermal frequency (ν) dependence of the complex AC susceptibility is defined in terms of real (χ') and imaginary (χ'') components following the equation

$$\chi(\nu) = \chi'(\nu) - i\chi''(\nu) \tag{3}$$

where

$$\chi' = \chi_\infty + \frac{\chi_0 - \chi_\infty}{1 + (\omega\tau)^2} \quad \text{and} \quad \chi'' = \frac{(\chi_0 - \chi_\infty)\omega\tau}{1 + (\omega\tau)^2} \tag{4}$$

χ_0 is the susceptibility at zero frequency (static approximation), χ_∞ is the susceptibility at the highest frequency, ω is $2\pi\nu$, and τ is the relaxation time.

A size distribution function, typically a log-normal function, must be introduced to take into account the different dimensions of the NPs:

$$p(r) = \frac{1}{\sqrt{2\pi}r\sigma} \exp\left\{\frac{-(\ln(r/r_m))^2}{2\sigma^2}\right\} \tag{5}$$

where r_m is the mean particle radius and σ is the standard deviation.

The physicomathematical model adopted here to fit the experimental susceptibility results is based on the sum of the two contributions (Néel and Brownian), both existing at room temperature. For both contributions, a different size distribution function has been used with a real (Néel) and hydrodynamic (Brownian) mean radius and standard deviation. The model has been proposed and extensively discussed in ref 19, and here only the results concerning all the different steps are presented.

5. DISCUSSION

The fluorescence spectra obtained for multifunctionalized magnetite NPs confirm the presence of the fluorescent molecules on the surface of the final structures. It is important to emphasize the following: (1) all the fluorescence analyses performed on the Fe_3O_4@SiO_2 NPs do not present, as expected, any fluorescence signal; (2) for all three PMPI coatings, a small but visible fluorescence peak is detected at the same wavelength (373 nm), probably due to the maleimidophenyl group, thus giving the fingerprint of the presence of the PMPI molecule; (3) the fluorescence features of the Fluo1, Fluo2, and Fluo3 molecules are mostly qualitatively reproduced in the spectra of the Fluo-coated NPs, suggesting that the functionalization reaction occurred in all samples. Nevertheless, small differences are found in the emission profiles of the anchored fluorophores. In detail, the two high-energy bands of the Fluo1 unbound molecule (372 and 392 nm) can be perfectly superimposed to the two corresponding peaks observed for the functionalized NPs, but the main fluorescence band at 494 nm is found to be totally quenched after the coupling. As already mentioned, this absence can be related to the small amount of Fluo1 on the final product (see Supporting Information). For the Fluo2 molecule, the peaks observed for the functionalized NPs (at 382 and 401 nm) completely agree with those observed for the Fluo2 molecule, at 384 and 402

dx.doi.org/10.1021/ic501194n | Inorg. Chem. 2014, 53, 9166−9173

nm, respectively. Finally, for the Fluo3 molecule we observe an incomplete agreement between our nanocarriers and the starting fluorescent molecule. Overall, these data suggest that the chemical structure and the loading of the fluorescent molecule can condition the emitting properties of the bound probes.

The qualitative analysis of the AC susceptibility data (both real and imaginary components) of the three different fluorescent nanocarriers are reported in Figures 5, 7, and 9 for the synthesis with Fluo1, Fluo2, and Fluo3 molecules, respectively. In these figures, the fits are represented as continuous lines. In Table 1 the results of the fit are summarized in terms of mean Brownian and Néel radii with the standard deviation related to the Brownian one. It is important to highlight that every step of the synthesis is correctly associated with an increase of the Brownian radius, as can be qualitatively seen by the shift to lower frequency of the imaginary peak. This result fits well with the reported fluorescence measurements since every change in the emission is associated with a change (increase) of the dimension.

Table 1. Mean Brownian and Néel Radii Obtained from Analysis of the AC Susceptibility Data for the Functionalization with the Different Fluorophores

sample	r_B[a] (nm)	σ[b]	mean Néel radius (nm)
Fe_3O_4@SiO_2	93	0.30	3.7
Fe_3O_4@SiO_2@PMPI	95	0.35	3.6
Fe_3O_4@SiO_2@PMPI@Fluo1	103	0.30	3.6
Fe_3O_4@SiO_2	83	0.32	3.5
Fe_3O_4@SiO_2@PMPI	95	0.30	3.6
Fe_3O_4@SiO_2@PMPI@Fluo2	100	0.30	3.5
Fe_3O_4@SiO_2	112	0.23	3.7
Fe_3O_4@SiO_2@PMPI	115	0.20	3.6
Fe_3O_4@SiO_2@PMPI@Fluo3	118	0.22	3.6

[a]Mean Brownian radius. [b]Standard deviation of r_B.

As already mentioned in section 3.1, every intermediate involved in the functionalization with molecule Fluo1 has been characterized also by DLS analysis. This technique allows obtaining dimensional information about the sample considering a completely different physical approach with respect to the AC susceptometry. The dimensions of the intermediates analyzed by the two techniques are reported in Table 2.

Table 2. Comparison of Mean Radii Obtained by AC Susceptibility and DLS Measurements

	r_m (nm)	
sample	AC susceptibility	DLS
Fe_3O_4@SiO_2	93	114
Fe_3O_4@SiO_2@PMPI	95	116
Fe_3O_4@SiO_2@PMPI@Fluo1	103	124

From Table 2 it is possible to observe a difference in the mean radius obtained using the above-mentioned techniques. Nevertheless, the gap between the values is constant for every intermediate (21 nm) and the increase in radius, related to each functionalization, is the same for AC susceptibility and DLS. Since the physical principles of the two experimental methods are strongly different, it is reasonable to obtain a mismatch between the results. Furthermore, to our knowledge, this is the first time that these two techniques are compared; more studies on the relation between the results and on the physical reason for the differences are now undergoing.

As mentioned in the section Magnetic Model, the fit of the experimental data has been obtained combining Brownian and Néel relaxations. These contributions give us the opportunity to collect simultaneously the dimension of the whole structure (Brownian) and the dimension of the internal magnetic core (Néel). Looking at the Néel values reported in Table 1, other important information can be achieved. In this case the value does not change during the synthesis, suggesting a stable radius around 3.6 nm. Considering the meaning of the Néel radius, i.e., the radius of the magnetic moiety of the structure, it is correct to obtain a constant value since the radius of the magnetite NPs is not affected by the surface functionalization. The obtained Néel radius is also in good agreement with our previous TEM analyses of Fe_3O_4 NPs and with our evaluation of the mean diameter (about 7 nm) from the Langevin fit of the room temperature hysteresis cycle.[21] Furthermore, the fit works well even when different solvents are used for the analysis, i.e., water for the SiO_2 coating and DMSO for the PMPI and Fluo1−Fluo3 coatings. In this case, the change of the solvent has to be considered in eq 2 by changing the viscosity from 1.005 mPa·s (H_2O) to 2.226 mPa·s (DMSO),[31] and considering the differing magnetic influence of the solvent.

It should be pointed out that no static magnetization data are presented here for the following reasons:

1. The zero field cooled (ZFC)−field cooled (FC) magnetization data strongly depend only on the real dimensions of the magnetic nucleus of the NPs and our distribution of magnetic nuclei is obviously the same through the different functionalization steps. Furthermore, this information can be easily achieved with the proposed dynamic method.

2. Static magnetic measurements by SQUID magnetometry must be obtained only after the sample centering protocol, performed at very low temperatures (typically around 30 K), i.e., a temperature where the solvents used are in the solid state, and this can affect the structure of the NPs or can destroy the sample holder.

The use of electron microscopy, both scanning and transmission, allowed achievement of not only morphological and dimensional information, but also the chemical composition of the products. For example, the presence of the organic functionalization with the fluorescent molecule for Fe_3O_4@SiO_2@PMPI@Fluo1 is confirmed by EDXS.

Furthermore, it is important to underline that electron microscopy and the AC susceptibility gave comparable results. Considering the intermediates involved in the synthesis with Fluo1, both Fe_3O_4@SiO_2 and Fe_3O_4@SiO_2@PMPI@Fluo1 present dimensions close to the values suggested by the magnetic behavior. The difference can be explained by two effects: the solvation of polar solvent molecules around the surface of the NP, and the agglomeration of NPs in solution due to magnetic dipole−magnetic dipole interactions.

These results confirm that the proposed magnetic analysis is an effective and powerful tool to achieve a quantitative description of the size distribution of NPs despite the nature of the functionalization pathway. Even if our three fluorescent molecules fall in the same (violet) fluorescence range, our suggested protocol can be easily adopted for other fluorescent moieties with stronger applicative properties: the functionaliza-

dx.doi.org/10.1021/ic501194n | Inorg. Chem. 2014, 53, 9166−9173

tion of magnetite NPs with yellow fluorescent or green fluorescent molecules is in progress.

6. CONCLUSIONS

An accurate and detailed protocol for the synthesis of magnetic nanoparticles functionalized with fluorescent molecules has been developed in our laboratory and successfully tested with three different organic fluorophores.

Two techniques based on different physical principles (fluorescence spectroscopy and AC magnetic susceptibility) have been used to accurately follow the different steps of the synthetic process. In order to validate the two technique approach, the intermediates involved in the functionalization with one fluorescent molecule have been also characterized with more conventional techniques, such as transmission electron microscopy, energy dispersive X-ray spectroscopy, and dynamic light scattering. The data obtained from all the techniques are in good agreement, validating the use of AC susceptibility and spectrofluorimetry to characterize the different intermediates involved in the synthesis.

Furthermore, the comparison between these two techniques allows highlighting the effectiveness of the proposed model for AC susceptibility analyses in multistep syntheses. The results disclose that from dynamic magnetic measurements it is possible to obtain both the dimension of the whole structure and the dimension of the internal magnetic portion simultaneously for each intermediate. To our knowledge this is the first time that AC susceptibility has been used to obtain dimensional information on each intermediate involved in a multistep process. The importance of the obtained result is besides increased since the proposed dynamic method can be used for any kind of functionalization and it is not related to specific characteristics of the used molecules.

In our opinion, these results bring a significant contribution to the field of multifunctionalized magnetic NPs, introducing an innovative, versatile, and fast method for the dimensional characterization of magnetic nanostructures in solution regardless of their nature.

■ ASSOCIATED CONTENT

Supporting Information

ESI-TOF HRMS, ^{1}H NMR, and ^{13}C NMR spectra of molecules Fluo1 and Fluo2. gHSQC of Fluo2. Fluorescence spectra of Fluo1 with respect to the concentration of the molecule. This material is available free of charge via the Internet at http://pubs.acs.org.

■ AUTHOR INFORMATION

Corresponding Author

*E-mail: mattia.lucchini@unige.it.

Notes

The authors declare no competing financial interest.

■ ACKNOWLEDGMENTS

The Italian Education, University and Research Ministry (MIUR) through the Research Project PRIN2011—NANOMED is gratefully acknowledged. The University of Genoa through the 2012 PRA project is also acknowledged. Thanks are due to Dr. G. Damonte (DIMES, Dipartimento di Medicina Sperimentale, and CEBR, Center of Excellence for Biomedical Research, University of Genoa) for running the HRMS experiments. For DLS measurements, Prof. Ranieri Rolandi is gratefully acknowledged.

■ REFERENCES

(1) Bell, A. T. *Science* **2003**, *299*, 1688−1691.
(2) Mondloch, J. E.; Bayram, E.; Fincke, R. G. *J. Mol. Catal. A* **2012**, *355*, 1−38.
(3) Paramsothy, M.; Tan, X. H.; Chan, J.; Kwok, R.; Gupta, M. *ISRN Nanomater.* **2012**, No. 169850.
(4) *Self-cleaning buildings*? 2012. http://www.alcoa.com/aap/north_america/pdf/ecoclean/EcoClean_Newsletter2.pdf.
(5) Tiwari, D. K.; Behari, J.; Sen, P. *World Appl. Sci. J.* **2008**, *3*, 417−433.
(6) Urban, I.; Ratckiffe, N. M.; Duffield, J. R.; Elder, G. R.; Patton, D. *Chem. Commun.* **2010**, *6*, 4583−4585.
(7) Zhong, C. J.; Luo, J.; Fang, B.; Wanjala, B. N.; Njoki, P. N.; Loukrakpam, R.; Yin, J. *Nanotechnology* **2010**, *21*, 062001.
(8) Yin, Y. X.; Wan, L.; Guo, Y. *Chin. Sci. Bull.* **2012**, *57*, 4104−4110.
(9) Popov, A. P.; Lademann, J.; Priezzhev, A. V.; Myllyla, R. *J. Biomed. Opt.* **2005**, *10*, 064037.
(10) Jaroenworaluck, A.; Sunsaneeyametha, W.; Kosachan, N.; Stevens, R. *Surf. Interface Anal.* **2006**, *38*, 473−477.
(11) *Nanoparticle Technology for Drug Delivery*; Gupta, R. B., Kompella, U. B., Eds.; Drugs and the Pharmaceutical Sciences 159; Taylor & Francis: New York, 2006.
(12) *Multifunctional Nanoparticles for Drug Delivery Applications: Imaging, Targeting, and Delivery*; Svenson, S., Prud'homme, R. K., Eds.; Springer: New York, 2012.
(13) Lee, D. E.; Koo, H.; Sun, I.; Ryu, J. H.; Kim, K.; Kwon, I. C. *Chem. Soc. Rev.* **2012**, *41*, 2656−2672.
(14) Jain, S.; Hirst, D. G.; O'Sullivan, J. M. *Br. J. Radiol.* **2012**, *85*, 101−113.
(15) Alexis, F.; Pridgen, E. M.; Langer, R.; Farokhzad, O. C. *Handb. Exp. Pharmacol.* **2010**, *197*, 55−86.
(16) He, R.; You, X.; Shan, J.; Gao, F.; Pan, B.; Cui, D. *Nanotechnology* **2007**, *18*, 315601.
(17) Corr, A.; Rakovich, Y. P.; Gun'ko, Y. K. *Nanoscale Res. Lett.* **2008**, *3*, 87−104.
(18) Ren, C.; Li, J.; Liu, Q.; Ren, J.; Chen, X.; Hu, Z.; Xue, D. *Nanoscale Res. Lett.* **2008**, *3*, 496−501.
(19) Lucchini, M. A.; Riani, P.; Canepa, F. *J. Nanopart. Res.* **2013**, *15*, 1601.
(20) Jadhav, S. A. *Cent. Eur. J. Chem.* **2012**, *10*, 295−299.
(21) Riani, P.; Napoletano, M.; Canepa, F. *J. Nanopart. Res.* **2011**, *13*, 7013−7020.
(22) Stober, W.; Fink, A.; Bohn, E. *J. Colloid Interface Sci.* **1968**, *26*, 62−69.
(23) Annunziato, M. E.; Patel, U. S.; Ranade, M.; Palumbo, P. S. *Bioconjugate Chem.* **1993**, *4*, 212−218.
(24) Lucchini, M. A.; Canepa, F. *J. Nanopart. Res.* **2012**, *14*, 809−816.
(25) Kalyanasundaram, K.; Thomas, J. K. *J. Am. Chem. Soc.* **1977**, *99*, 2039−2044.
(26) Ipe, B. I.; Thomas, K. G. *J. Phys. Chem. B* **2004**, *108*, 13265−13272.
(27) Néel, L. *C. R. Acad. Sci.* **1949**, *228*, 664−668.
(28) Frenkel, J. *The Kinetic Theory of Liquids*; Dover Publications: New York, 1955.
(29) Debye, P. *Polar Molecules*; Chemical Catalog Co., Inc.: New York, 1929.
(30) Fannin, P. C.; Coffey, W. T. *Phys. Rev. E* **1995**, *52*, 6129−6140.
(31) Omota, L. M.; Iulian, O.; Ciocîrlan, O.; Niţă, I. *Rev. Roum. Chim.* **2008**, *53*, 977−988.